Calsarcin-2 deficiency increases exercise capacity in mice through calcineurin/NFAT activation

Norbert Frey, … , Hugo A. Katus, Eric N. Olson

Research Article

The composition of skeletal muscle, in terms of the relative number of slow- and fast-twitch fibers, is tightly regulated to enable an organism to respond and adapt to changing physical demands. The phosphatase calcineurin and its downstream targets, transcription factors of the nuclear factor of activated T cells (NFAT) family, play a critical role in this process by promoting the formation of slow-twitch, oxidative fibers. Calcineurin binds to calsarcins, a family of striated muscle–specific proteins of the sarcomeric Z-disc. We show here that mice deficient in calsarcin-2, which is expressed exclusively by fast-twitch muscle and encoded by the myozenin 1 (*Myoz1*) gene, have substantially reduced body weight and fast-twitch muscle mass in the absence of an overt myopathic phenotype. Additionally, *Myoz1* KO mice displayed markedly improved performance and enhanced running distances in exercise studies. Analysis of fiber type composition of calsarcin-2–deficient skeletal muscles showed a switch toward slow-twitch, oxidative fibers. Reporter assays in cultured myoblasts indicated an inhibitory role for calsarcin-2 on calcineurin, and *Myoz1* KO mice exhibited both an excess of NFAT activity and an increase in expression of regulator of calcineurin 1-4 (RCAN1-4), indicating enhanced calcineurin signaling in vivo. Taken together, these results suggest that calsarcin-2 modulates exercise performance in vivo through regulation of calcineurin/NFAT activity and subsequent alteration of the fiber type composition of skeletal muscle.

Find the latest version:

https://jci.me/36277/pdf

Calsarcin-2 deficiency increases exercise capacity in mice through calcineurin/NFAT activation

Norbert Frey,[1] Derk Frank,[1] Stefanie Lippl,[1] Christian Kuhn,[1] Harald Kögler,[2] Tomasa Barrientos,[3] Claudia Rohr,[1] Rainer Will,[1] Oliver J. Müller,[1] Hartmut Weiler,[4] Rhonda Bassel-Duby,[3] Hugo A. Katus,[1] and Eric N. Olson[3]

[1]Department of Internal Medicine III, University of Heidelberg, Heidelberg, Germany. [2]Department of Cardiology and Pneumology, University of Göttingen, Göttingen, Germany. [3]Department of Molecular Biology, University of Texas Southwestern Medical Center, Dallas, Texas, USA. [4]Blood Research Institute, BloodCenter of Wisconsin, Milwaukee, Wisconsin, USA.

The composition of skeletal muscle, in terms of the relative number of slow- and fast-twitch fibers, is tightly regulated to enable an organism to respond and adapt to changing physical demands. The phosphatase calcineurin and its downstream targets, transcription factors of the nuclear factor of activated T cells (NFAT) family, play a critical role in this process by promoting the formation of slow-twitch, oxidative fibers. Calcineurin binds to calsarcins, a family of striated muscle–specific proteins of the sarcomeric Z-disc. We show here that mice deficient in calsarcin-2, which is expressed exclusively by fast-twitch muscle and encoded by the myozenin 1 (*Myoz1*) gene, have substantially reduced body weight and fast-twitch muscle mass in the absence of an overt myopathic phenotype. Additionally, *Myoz1* KO mice displayed markedly improved performance and enhanced running distances in exercise studies. Analysis of fiber type composition of calsarcin-2–deficient skeletal muscles showed a switch toward slow-twitch, oxidative fibers. Reporter assays in cultured myoblasts indicated an inhibitory role for calsarcin-2 on calcineurin, and *Myoz1* KO mice exhibited both an excess of NFAT activity and an increase in expression of regulator of calcineurin 1-4 (RCAN1-4), indicating enhanced calcineurin signaling in vivo. Taken together, these results suggest that calsarcin-2 modulates exercise performance in vivo through regulation of calcineurin/NFAT activity and subsequent alteration of the fiber type composition of skeletal muscle.

Introduction

The ubiquitously expressed serine/threonine phosphatase calcineurin plays a critical role in the remodeling of striated muscle tissue (reviewed in ref. 1). Low amplitude, sustained calcium waves induce calcium binding to calmodulin, which in turn associates with the regulatory calcineurin B subunit, thereby activating calcineurin A (2). Activated calcineurin A dephosphorylates transcription factors of the nuclear factor of activated T cells (NFAT) family, leading to their nuclear translocation. In skeletal muscle, nuclear NFATs associate with other transcription factors such as myocyte enhancer factor 2 (MEF2) and activate a characteristic Ca^{2+}-dependent gene expression program (1, 3, 4). The activation of calcineurin/NFAT specifically induces a muscle fiber type switch toward a slow-twitch and oxidative phenotype, with an increase in expression of a subset of genes associated with type I myofibers, such as *myoglobin* and *troponin I slow* (5, 6), allowing for sustained and fatigue-resistant muscle activity. In contrast, high-frequency nerve activity promotes the formation of fast-twitch, glycolytic type IIb fibers, thereby facilitating quick contractions with rapid fatigability. In genetically engineered mice, forced overexpression of calcineurin in skeletal muscle induces an increase in the number of slow-twitch muscle fibers (7), while genetic disruption of calcineurin Aα or Aβ leads

to a significant decrease in slow-twitch, oxidative fibers. Likewise, skeletal muscle–specific calcineurin B1–null mice fail to upregulate slow-twitch fibers upon increased workload (8).

In an attempt to identify novel muscle-specific modulators of calcineurin activity, we previously performed a yeast 2-hybrid assay using the regulatory subunit of calcineurin A as bait. With this approach, we discovered a family of striated muscle–specific, calcineurin-binding proteins, the calsarcins (9), which localize to the Z-disc of the sarcomere (reviewed in ref. 10). The calsarcin family consists of 3 members, with calsarcin-2 (also termed "myozenin 1" [Myoz1; ref. 11], or "FATZ" [ref. 12]) and calsarcin-3 being exclusively expressed in fast-twitch fibers of skeletal muscle tissue (9, 13). In contrast, calsarcin-1 is expressed in the adult heart and in slow-twitch fibers of skeletal muscle. Calsarcins are hallmarked by a multitude of Z-disc interaction partners that, in addition to calcineurin, include α-actinin, LIM domain–binding 3 (LDB3, also known as Cypher, ZASP, and Oracle), Telethonin/T-cap, γ-filamin (9, 13), and myotilin (14). Targeted ablation of the *Myoz2* allele sensitized calsarcin-1–deficient mouse hearts to pressure overload and chronic calcineurin activation with excessive hypertrophy and subsequent cardiomyopathy (15), while transgenic overexpression of calsarcin-1 protected mouse hearts from angiotensin II–induced cardiac hypertrophy (16). In slow-twitch skeletal muscle, the lack of calsarcin-1 led to an increase in calcineurin activity associated with an expansion of type I muscle fibers (15).

To determine the function of calsarcins in fast-twitch skeletal muscle in vivo, we generated mice with genetic ablation of the fast-twitch muscle isoform calsarcin-2. Compared with WT mice,
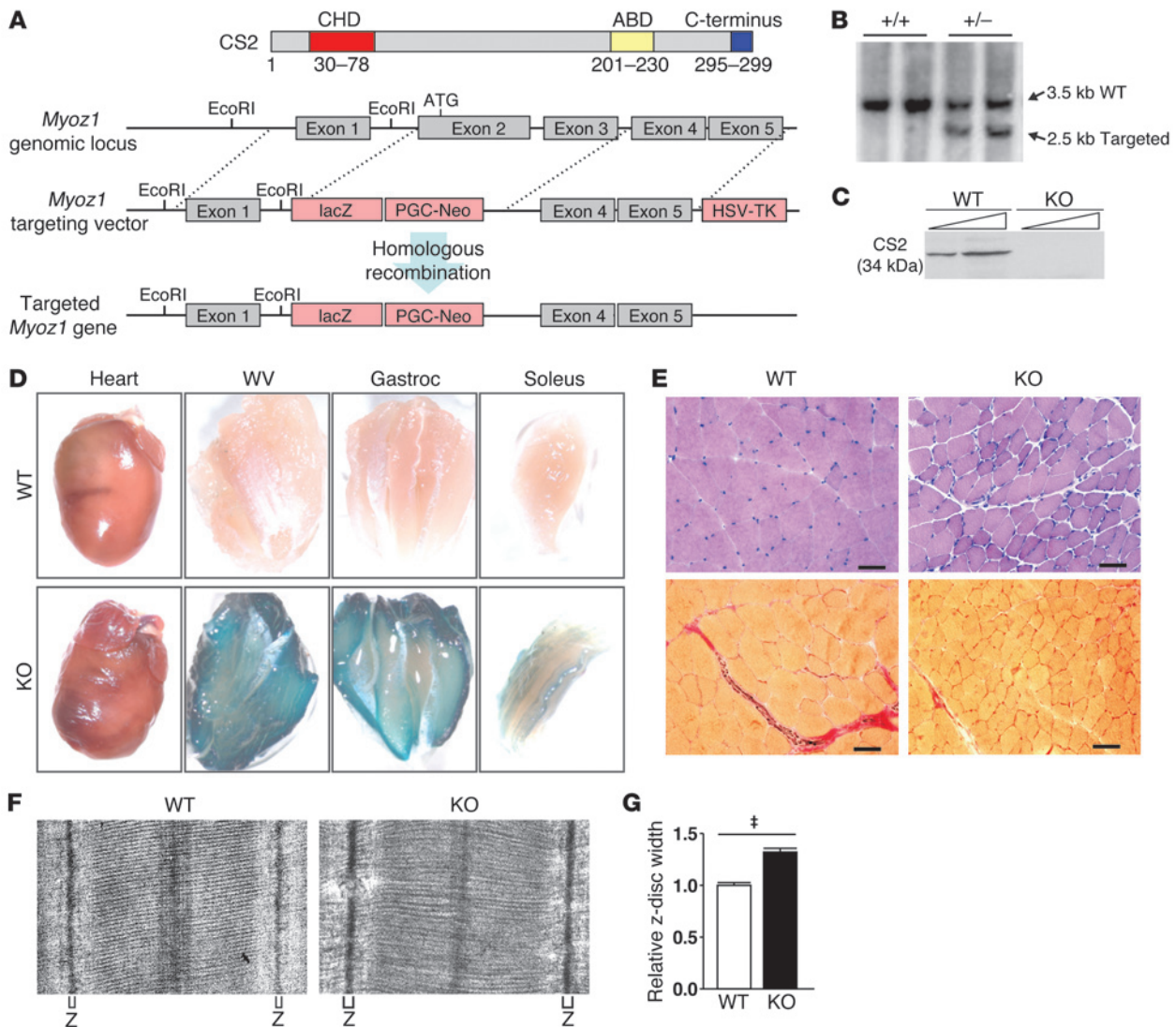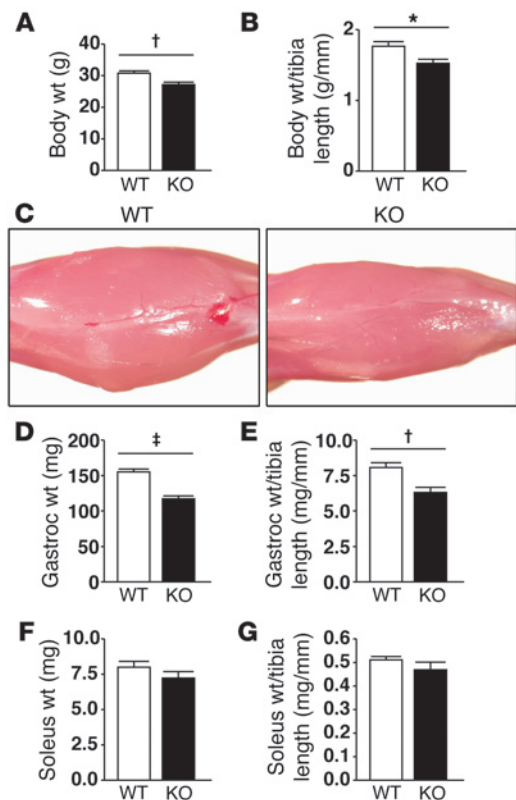
Figure 1
Generation of *Myoz1* mutant mice. (**A**) Schematic protein structure of calsarcin-2 highlights the calsarcin homology domain (CHD), which is highly conserved between calsarcin isoforms, the α-actinin binding domain (ABD), and the C terminus, which is highly homologous throughout the calsarcin family. The targeting vector and the targeted mouse *Myoz1* allele are shown. Homologous recombination resulted in the deletion of exon 2 and 3 in the *Myoz1* gene and their replacement with a neomycin-lacZ reporter cassette. CS2, calsarcin-2. (**B**) Southern blot analysis of EcoRI-digested genomic DNA of the F1 generation of *Myoz1*$^{-/+}$ mice. The 3.5-kb band represents the WT allele, and the 2.5-kb band corresponds to the targeted allele. (**C**) Western blot of muscle protein homogenate (50 and 150 μg) from gastrocnemius of WT and *Myoz1* KO mice. (**D**) β-Galactosidase staining of tissues from WT and *Myoz1* KO animals. The calsarcin-2–deficient tissues showed strong staining in predominantly fast-twitch fiber–containing muscles (e.g., white vastus [WV], gastrocnemius [gastroc]). The soleus, a predominantly slow-twitch muscle, displayed staining in a minor subset of fibers. The heart showed no significant expression of *Myoz1*. Original magnification, ×4. (**E**) H&E staining (top) and van Giesson staining (bottom) of gastrocnemius from *Myoz1* KO mice and WT littermates. Scale bars: 50 μm. (**F**) Electron microscopy photographs of gastrocnemius (original magnification, ×19,000). (**G**) Quantification of 100 Z-disc widths from $n = 4$ mice per genotype. ‡$P < 0.001$.

calsarcin-2–deficient mice displayed a significantly reduced body weight as well as a decreased fast-twitch muscle mass. Muscle atrophy does not account for the reduced muscle weight, as *Myoz1* KO mice displayed markedly increased running distances in voluntary running as well as in a forced treadmill setting. Fiber type composition analyses of skeletal muscles revealed a significant switch toward oxidative fibers, with a substantial increase in type IIA fibers in fast-twitch muscles, consistent with an increase in calcineurin activity. In fact, skeletal muscles of mice lacking calsarcin-2

showed a significant excess of calcineurin activity compared with WT controls. Our data suggest an essential role for calsarcin-2 in the regulation of fiber type composition as well as exercise tolerance of skeletal muscle, likely via modulation of calcineurin-dependent signaling.

Results

Generation of Myoz1 mutant mice. To analyze the function of calsarcin-2 in vivo, we generated mice with germline deletion of the

Figure 2
Reduced body weight and fast-twitch muscle mass in *Myoz1*-deficient mice. (**A**) Significant reduction in body weight of *Myoz1* KO mice (*n* = 13–15) and (**B**) in body weight normalized to tibia length in *Myoz1* KO mice (*n* = 6). (**C**) Morphology of skinned hindlimbs of *Myoz1* KO mouse, revealing a slimmer shape of the calf in *Myoz1* KO mice compared with WT littermate. Original magnification, ×4. (**D**) Weight of gastrocnemius in *Myoz1* KO mice compared with WT littermates (*n* = 13–15). (**E**) Gastrocnemius mass normalized to tibia length (*n* = 6). (**F**) Weight of soleus in *Myoz1* KO mice compared with WT controls. (**G**) Soleus weight normalized to tibia length. *$P < 0.05$, †$P < 0.01$, ‡$P < 0.001$.

Myoz1 allele by replacing exons 2 (which contains the translational start) and 3 with a neomycin resistance cassette and a lacZ reporter gene (Figure 1A). Breeding of *Myoz1* mutant mice resulted in the expected Mendelian ratios of offspring. Genotyping was performed by Southern blot analysis and/or PCR (Figure 1B). The absence of calsarcin-2 expression was confirmed in *Myoz1* KO mice by western blot analysis using protein homogenates of the gastrocnemius, a predominantly fast-twitch muscle. As expected, WT mice expressed calsarcin-2 protein, while no calsarcin-2 protein was detectable in *Myoz1* KO mice (Figure 1C). The in vivo expression pattern of the *Myoz1* gene was determined using β-galactosidase staining to detect the lacZ reporter under the control of the endogenous *Myoz1* promoter (Figure 1D). These experiments revealed strong expression of *Myoz1* in predominantly fast-twitch muscles, such as white vastus and gastrocnemius. In contrast, the soleus, a predominantly slow-twitch muscle, showed low *Myoz1* expression confined to a subset of myofibers. The adult myocardium was devoid of *Myoz1* expression, consistent with our previous observations (9).

No obvious signs of myopathy were detected in the skeletal muscle of *Myoz1*-deficient mice by light microscopy (Figure 1E). However, by electron microscopy we found a widening of Z-discs (Figure 1, F and G), similar to previous findings in hearts of *Myoz2*-deficient mice (15).

Myoz1-deficient mice display a reduction in body weight and fast-twitch muscle mass. *Myoz1* KO mice were viable, fertile, showed no overt abnormalities, and had a normal life span of greater than 20 months without premature death. However, morphometric analyses revealed a significant reduction in body weight in *Myoz1* KO mice (*P* = 0.0017; Figure 2A). This effect remained significant when normalizing body weight to tibia length, thereby excluding a global growth retardation phenotype (*P* = 0.018; Figure 2B). Sub-

sequent analyses of the gross morphology of skinned hindlimbs of *Myoz1* KO mice uncovered a considerably slimmer shape of the calf compared with WT (Figure 2C). Of note, the silhouette of the calf is chiefly modeled by the gastrocnemius, whereas the soleus only marginally contributes to the shape of the calf. To further characterize this morphological difference, we weighed individual hindlimb muscles. The gastrocnemius of *Myoz1* KO animals showed a 24.4% weight reduction compared with the gastrocnemius of WT littermates (*P* < 0.0001; Figure 2D). Normalization to body weight or tibia length (*P* = 0.0066; Figure 2E) did not change the level of significance. Interestingly, when comparing the weight of the soleus, a slow-twitch muscle with low expression levels of calsarcin-2, no difference was observed between *Myoz1* KO and WT mice (Figure 2, F and G).
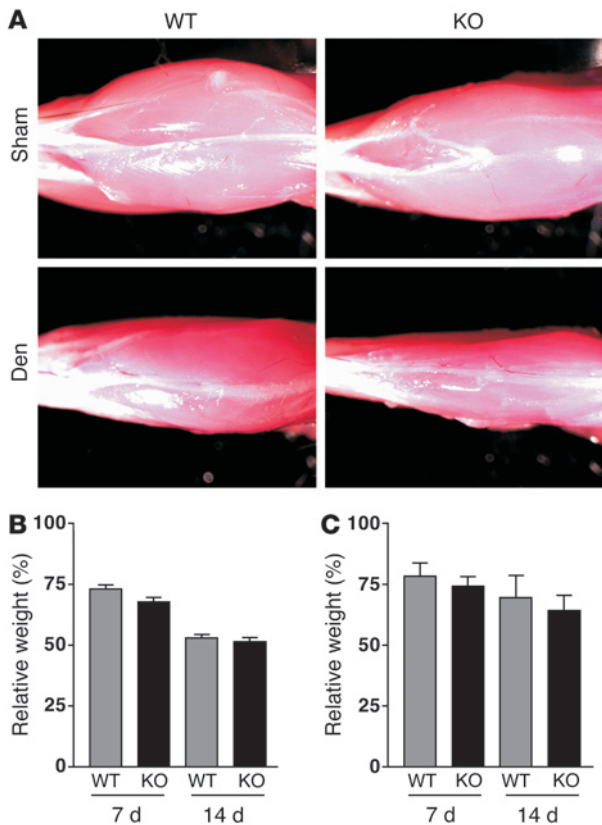
Lack of enhanced muscle atrophy in Myoz1-deficient mice. A common cause of muscle weight loss is atrophy, a process which accounts for the progressive muscle loss during immobilization, denervation or severe systemic diseases like AIDS, heart failure, or cancer (17). To test whether atrophy accounted for the reduced muscle weight observed in *Myoz1* KO animals, we performed denervation experiments by severing the sciatic nerve, which leads to progressive atrophy of the gastrocnemius, soleus, and tibialis anterior, as measured by a reduction in muscle mass. As expected, both *Myoz1* KO and WT mice showed substantial atrophy upon denervation (Figure 3A), but no substantial differences in the relative degree of atrophy were detectable between KO and WT mice. The relative gastrocnemius weight loss in *Myoz1* KO mice after 7 days was 32.3%, while WT littermates lost 26.9% in muscle weight. After 14 days, *Myoz1* KO mice lost 48.5% of gastrocnemius weight compared with 47.0% in WT muscle (Figure 3B). Weight loss of the soleus of *Myoz1* KO and WT mice also did not differ significantly (Figure 3C). After one week, *Myoz1* KO mice had lost 25.5% of muscle mass, compared with 21.6% in WT mice. After 2 weeks, the soleus weight loss was 35.7% in *Myoz1* KO, while the soleus of similarly treated WT animals lost 30.3% of its weight. Thus, following denervation, mice lacking calsarcin-2 showed no differential degree of atrophy compared with WT mice in either fast-twitch and slow-twitch muscles. Hence, a marked contribution of atrophic processes to the baseline weight loss of muscles lacking calsarcin-2 appears unlikely.

Ablation of calsarcin-2 increases endurance capacity. To determine whether ablation of calsarcin-2 leads to impaired muscle function, we analyzed intact diaphragm muscle strips for fatigability and tension power (Figure 4, A and B). Calsarcin-2 is highly expressed in the diaphragm. Surprisingly, both analyses showed greater resistance to fatigue as well as greater tension power upon tetanic stimulations in *Myoz1* KO muscles. To further analyze this finding

Figure 3
Lack of enhanced muscle atrophy in *Myoz1*-deficient mice. (**A**) Following denervation (den) or sham operation, atrophy of the hindlimb muscles was observed in both WT and *Myoz1* KO mice after 2 weeks Original magnification, ×4. (**B** and **C**) Weight of gastrocnemius (**B**) and soleus (**C**) showed no significant differences between *Myoz1* KO mice and WT littermates after 1 or 2 weeks following denervation (*n* = 5 each).

reduced body weight (*P* = 0.061; Figure 4E). Similar to the observations in sedentary mice, the mass of the gastrocnemius remained significantly reduced (*P* = 0.0001; Figure 4F) independent of normalization to body weight (*P* = 0.002; Figure 4G). Again, the weight of the soleus was comparable in both *Myoz1* KO and WT control mice (data not shown).

Given that endurance is fundamentally based on the available amount of oxidative capacity, these findings suggest that *Myoz1*-deficient mice display an increased oxidative capacity in their skeletal muscles. To further test this hypothesis, we used a treadmill to run mice to exhaustion. Mice were forced to run according to a defined protocol (10% incline, 10 minutes at 10 m/min, with an increase of an additional 2 m/min every 2 minutes [+0.033 m/s]). This experimental design is known to rapidly reach the point at which the oxidative threshold is exceeded (18). Consistently, *Myoz1* KO mice displayed a significantly extended endurance capacity compared with WT littermates (*P* = 0.027; Figure 5A). The *Myoz1* KO mice ran 1,511 seconds (25.2 minutes) to exhaustion, while WT mice only ran for a mean of 982 seconds (16.4 minutes). This enhanced performance corresponds to a distance of 435.8 m in *Myoz1* KO mice compared with 248.7 m in WT mice (*P* = 0.027; Figure 5B) and to an energy expenditure of 24.8 joules and 13.9 joules, respectively (*P* = 0.024; Figure 5C). We conclude that lack of calsarcin-2 markedly increases the endurance capacity of mice under both voluntary and forced conditions.

Myoz1 KO mice display a fiber type shift toward slow-twitch oxidative fibers. Skeletal muscles are composed of a spectrum of different fibers, ranging from ultra-fast glycolytic type IIb fibers to slow, oxidative, fatigue-resistant type I fibers. The range between these

in vivo, we compared the voluntary running behavior of *Myoz1* KO mice with that of their WT littermates. Mice were provided unlimited access to running wheels, and after 1 week of acclimatization, data were acquired for 14 days. Unexpectedly, *Myoz1* KO mice ran considerably longer distances per day (*P* = 0.033; Figure 4C) and reached higher average speeds (*P* = 0.036; Figure 4D) compared with WT littermates. Of note, even after 14 days of running, animals lacking calsarcin-2 still displayed a strong tendency toward

Figure 4
Ablation of calsarcin-2 increases endurance capacity following voluntary running wheel exercise. Diaphragm muscle strip analyses of *Myoz1* KO mice compared with WT controls showed (**A**) less fatigability (–13.8%; *P* < 0.0001) (100 Hz/250 ms) and (**B**) greater tension power upon tetanic stimulations (+13.4%; *P* = 0.011). (**C**) Increases were observed in daily running distances (*n* = 8 each) and (**D**) average speeds (*n* = 8 per group) of *Myoz1* KO mice compared with WT littermates. Changes were also observed in (**E**) body weight (*n* = 8), (**F**) gastrocnemius weight (*n* = 8), and (**G**) gastrocnemius mass normalized to body weight (*n* = 8) of *Myoz1* KO mice and WT littermates after 14 days of running. *P* < 0.05, †*P* < 0.01, ‡*P* < 0.001.
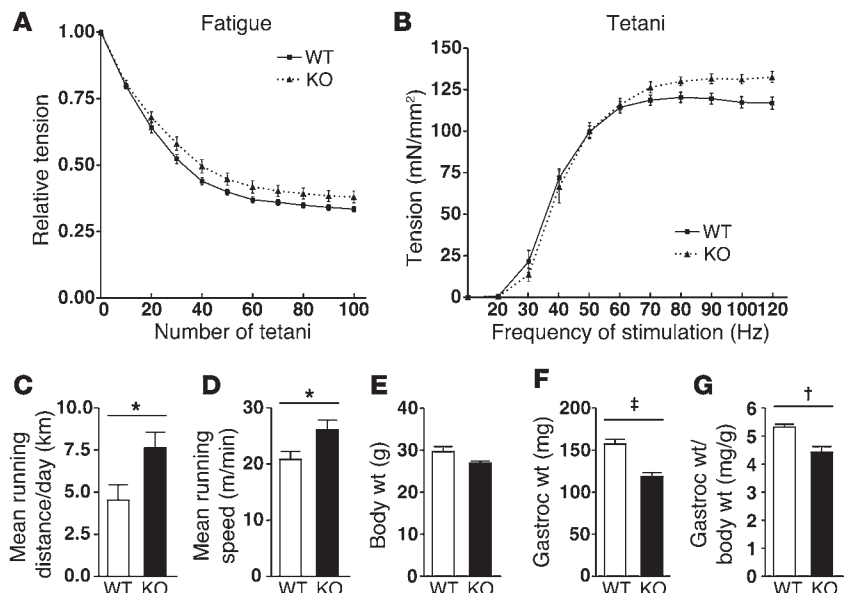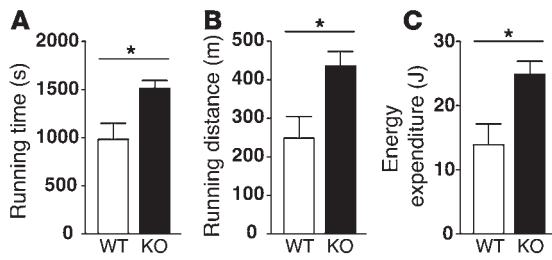
Figure 5
Ablation of calsarcin-2 increases endurance capacity after treadmill running. (**A**) *Myoz1* KO mice ran 1,511 seconds (25.2 min) to exhaustion, while WT mice ran for a mean of 982 seconds (16.4 min, *n* = 5–6). (**B**) *Myoz1* KO mice ran a distance of 435.8 m, compared with WT mice, which ran 248.7 m (*n* = 5–6). (**C**) *Myoz1* KO mice spent 24.8 joules while running, compared with WT littermates, which used 13.9 joules (*n* = 5–6). *P < 0.05.

extreme fiber types is complemented by IIx and IIa fibers, which reveal an intermediary phenotype. While fiber types I and IIa exhibit an oxidative metabolism, type IIx and IIb fibers bear glycolytic capacities (1, 19, 20). To elucidate the morphological and molecular basis of the increased endurance capacity of *Myoz1* KO mice, we analyzed the fiber composition of gastrocnemius (predominantly fast-twitch) and soleus (predominantly slow-twitch) muscles.

Interestingly, *Myoz1* KO mice exhibited a considerable excess of oxidative type IIa fibers in the gastrocnemius (Figure 6A). When

quantifying and normalizing this effect per mm^2, we found a 56.2% increase of type IIa fibers in *Myoz1* KO mice compared with WT littermates (*P* = 0.01; Figure 6B), while the cross-sectional area of individual type IIa fibers remained unchanged (Figure 6C).

We examined whether the number of fibers staining positive for succinate dehydrogenase (SDH) also differed between *Myoz1* KO and WT controls. SDH is localized to the inner membrane of the mitochondria and takes part in the Krebs cycle. Therefore, it can be used as an indicator for oxidative fibers (Supplemental Figure 1; supplemental material available online with this article; doi:10.1172/JCI36277DS1). Consistent with the markedly increased number of type IIa fibers, the content of fibers staining positive for SDH was significantly higher in the gastrocnemius of *Myoz1* KO mice (Figure 6D). When quantifying SDH-positive fibers, we found a 2.6-fold increase in *Myoz1* KO mice (*P* = 0.008; Figure 6E), confirming an enhanced oxidative capacity in calsarcin-2–deficient gastrocnemius muscles.

Conversely, the glycolytic fast-twitch and fatigue-susceptible type IIb fibers (Figure 6F) were increased in number per mm^2 (*P* = 0.0007; Figure 6G) but substantially reduced in size (*P* = 0.0001; Figure 6H). The mean total muscle cross-sectional area of gastrocnemius muscle was reduced as well (78.7%, *P* < 0.05; Supplemental Figure 2). Thus, the increase in number per mm^2 can be explained by a compaction of muscle fibers, while the total amount of type IIb fibers remained unchanged. Immunofluorescence analyses of soleus muscle (Figure 6I) revealed a highly significant increase of 68.1% in the number of type I fibers in *Myoz1* KO mice (*P* = 0.007; Figure 6J). Interestingly,

Figure 6
Fiber type shift seen in skeletal muscle of *Myoz1* KO mice. (**A**) Immunofluorescence histochemistry for type IIa fibers using SC-71 antibody (green, FITC-labeled lectin). (**B**) An increase of 56.2% was found in the number of type IIa fibers/mm^2 in the gastrocnemius of *Myoz1* KO mice compared with WT littermates (*n* = 6–7 animals). (**C**) The cross-sectional area of type IIa fibers remained unchanged. (**D**) SDH staining of gastrocnemius showed an increase of SDH-positive fibers in *Myoz1* KO mice compared with WT controls. (**E**) Quantification of SDH-positive fibers shows a 2.58-fold increase in *Myoz1* KO mice compared with WT (*n* = 4 mice per group). (**F**) Immunofluorescence histochemistry for type IIb fibers using BF-F3 antibody (green, FITC-labeled lectin). (**G**) The number of type IIb fibers/mm^2 increased in *Myoz1* KO mice. (**H**) A reduction was found in the cross-sectional area of type IIb fibers (*n* = 105–178 cells). (**I**) Immunofluorescence histochemistry for type I fibers using NOQ7.5.4D antibody. (**J**) The number of type I fibers/mm^2 increased in the soleus of *Myoz1* KO mice compared with WT littermates (*n* = 4–6 mice). (**K**) Cross-sectional area of type I fibers increased in the soleus in *Myoz1* KO mice compared with WT controls (*n* = 143–260 fibers). Scale bars: 100 μm. *P < 0.05, †P < 0.01, ‡P < 0.001.
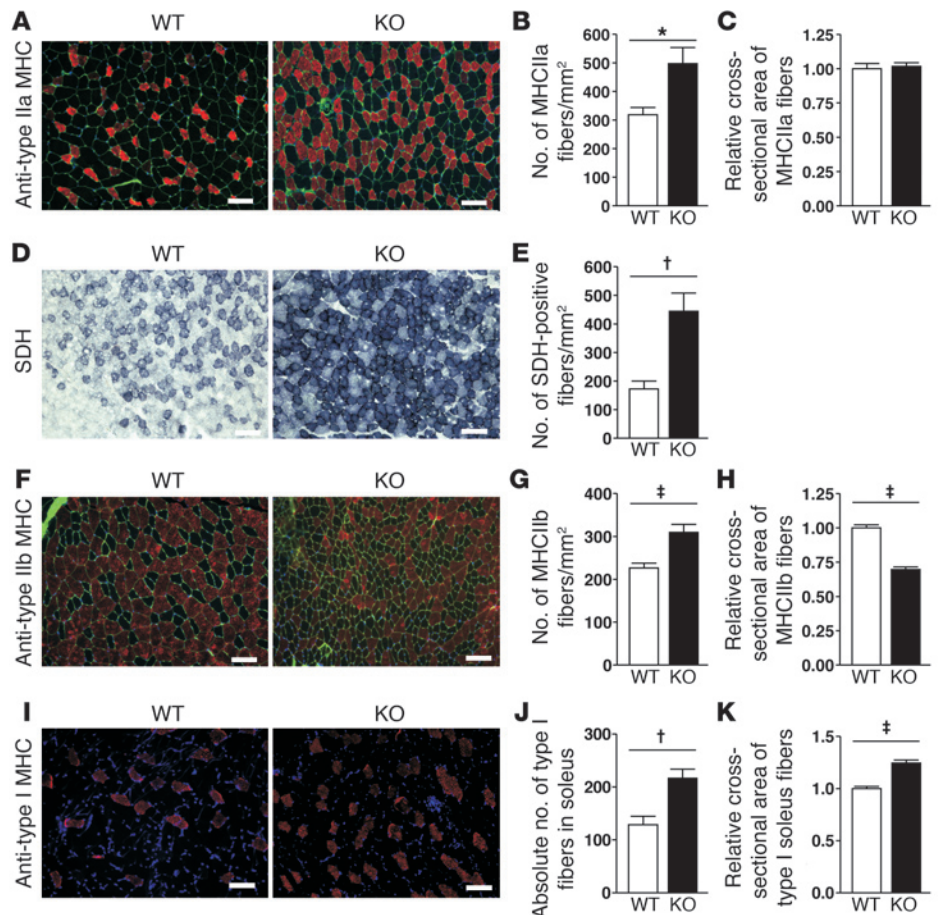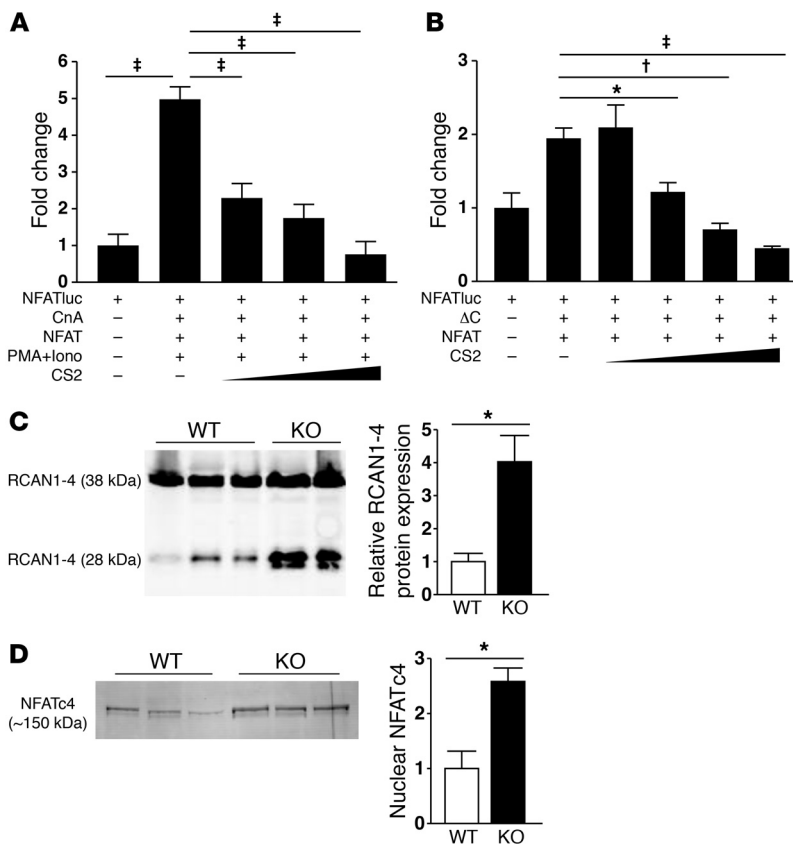
Figure 7

Calsarcin-2 inhibits calcineurin activity in vitro and in vivo. C2C12 cells containing an NFAT reporter plasmid (NFATluc) were transfected with (**A**) full-length calcineurin A (CnA), an NFAT expression plasmid, and an increasing amount of calsarcin-2 or (**B**) constitutively active calcineurin (ΔC) and NFAT expression plasmid, resulting in induction of the NFAT-luciferase reporter ($P < 0.01$). (**A**) After transfection, cells underwent treatment with the calcineurin stimulators PMA and ionomycin (PMA+Iono). PMA and ionomycin strongly induced NFAT reporter activity, while increasing amounts of calsarcin-2 completely abrogated the increase in reporter gene activity. (**B**) The presence of calsarcin-2 inhibited the calcineurin activity in a dose-dependent and significant manner. (**C**) Western blot analysis (left) and densitometric quantification (right) showing induction of the endogenous calcineurin-responsive *Rcan1-4* gene in *Myoz1* KO mice and (**D**) an increase of nuclear NFATc4 in the gastrocnemius of *Myoz1* KO mice compared with that of WT littermates. *$P < 0.05$, †$P < 0.01$, ‡$P < 0.001$.

the gain of slow-twitch fibers was further augmented by the finding that *Myoz1* KO type I fibers also featured a pronounced increase (24.6%) in cross-sectional area ($P < 0.0001$; Figure 6K), while the number of type IIa fibers remained unchanged (data not shown). Taken together, these findings show that the absence of calsarcin-2 leads to a marked fiber type shift towards oxidative, slow-twitch fibers, either via an increase of type IIa fibers (in fast-twitch muscles) or of type I fibers (in slow-twitch muscles).
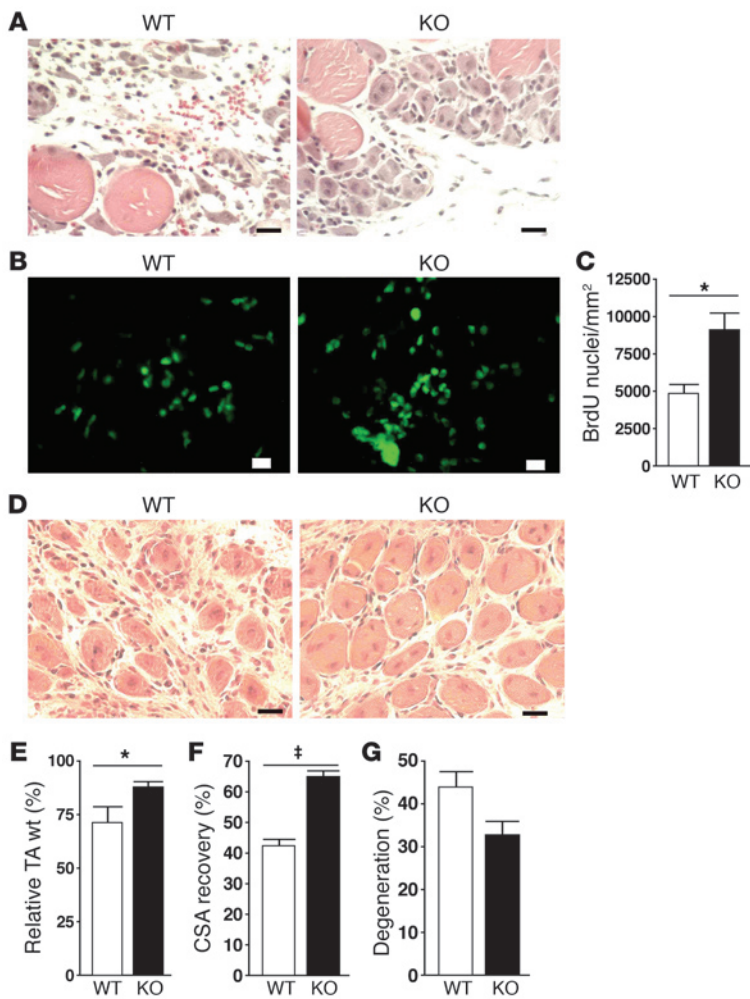
Calsarcin-2 inhibits calcineurin activity. The phosphatase calcineurin acts as a key regulator of fiber type specificity by promoting expression of a slow-twitch and oxidative phenotype with an increase of a subset of genes, which are associated with type I and type IIa myofibers (5, 6). We have previously shown that the absence of another member of the calsarcin family, calsarcin-1, which is exclusively expressed in slow-twitch muscle fibers and the heart (9), leads to an excess of calcineurin activity in these tissues (15). Since calsarcin-1 and calsarcin-2 both bind to calcineurin, we tested whether calsarcin-2 modulates calcineurin activity in C2C12 myoblasts stably transfected with an NFAT-responsive luciferase reporter (NFAT-luc). These cells were cotransfected with full-length (non–constitutively active) calcineurin A, an NFAT expression plasmid, and increasing dosages of calsarcin-2. Subsequently, cells were incubated with the known calcineurin stimulators PMA and ionomycin. PMA and ionomycin induced NFAT reporter activity 5.0-fold ($P < 0.001$; Figure 7A). In contrast, adding increasing amounts of calsarcin-2 completely abrogated the increase in reporter gene activity to values even lower than the unstimulated baseline level (75.8% of the baseline value), suggesting that calsarcin-2 inhibits calcineurin/NFAT signaling. More-

over, calsarcin-2 also inhibits baseline calcineurin/NFAT activity in C2C12 cells (Supplemental Figure 3).

To further corroborate these data, we examined whether calsarcin-2 is also capable of inhibiting constitutively activated calcineurin. NFAT-luc reporter cells were transfected with cDNAs encoding for constitutively active calcineurin (ΔC; ref. 21) and NFAT, resulting in a significant induction of the luciferase reporter ($P < 0.01$; Figure 7B). Again, the addition of calsarcin-2 completely inhibited the activation of the reporter gene.

Increased calcineurin activity in skeletal muscles of Myoz1 KO mice. Given the results from the in vitro experiments, we hypothesized that the loss of calsarcin-2 might cause an increase in calcineurin activity in vivo, which in turn would provide an explanation for the observed fiber type shift. To test this assumption, we examined the regulation of a calcineurin-dependent gene, regulator of calcineurin 1 (*Rcan1*; formerly termed modulatory calcineurin interacting protein [*Mcip1*] or Down syndrome candidate region 1 [*Dscr1*]; ref. 22), in gastrocnemius. Since the expression of the Rcan isoform 1-4 is tightly controlled by a cluster of 15 NFAT binding sites, it represents a sensitive endogenous calcineurin reporter gene (23). Consistent with an increase in calcineurin activity, Rcan1-4 was markedly induced in *Myoz1* KO mice (Figure 7C). Densitometric quantification of the western blot revealed a 4.0-fold upregulation of Rcan1-4 ($P = 0.02$; Figure 7C).

Another hallmark of calcineurin signaling is the dephosphorylation and consequent nuclear translocation of its downstream targets, transcription factors of the NFAT family (24). In *Myoz1* KO mice, the amount of nuclear NFATc4 was significantly increased ($P = 0.017$; Figure 7D). Densitometric analysis showed a signifi-

degenerated tissue (43.9% in WT vs. 32.7% in KO mice, $P = 0.05$; Figure 8G). Taken together, these data show that *Myoz1* KO mice have an enhanced capacity for skeletal muscle regeneration, similar to other mouse models with enhanced calcineurin activity.

Discussion

The results of this study show that calsarcin-2 negatively modulates calcineurin activity both in vitro and in vivo. Specifically, the genetic ablation of calsarcin-2 induced a significant fiber type shift toward more oxidative fibers with enhanced endurance (Figure 9). Based on these and earlier findings (9, 13, 15), we propose that calsarcin-2 serves a critical role in the regulation of muscle fiber composition and exercise performance in vivo.

A key finding in the current study is that calsarcin-2–deficient mice run faster and greater distances than their WT littermates. This "endurance phenotype" is accompanied by a reduction of body weight and fast-twitch muscle mass. Such a phenomenon has been observed in only a few other mouse models. For example, mice overexpressing the PPAR coactivators 1α and β (PGC-1α and -β; refs. 18, 28) as well as PPARδ (29) share the ability to strongly induce mitochondrial biogenesis and gene expression. Muscle-confined PGC-1α overexpression predominantly induced slow-twitch, oxidative type I and IIa fibers (28). Yet this overexpression cannot be solely responsible for type I fiber formation, since whole body *PGC-1α*–deficient mice show a normal distribution of fiber types (30). In contrast, PGC-1β, a close relative of PGC-1α, drives the formation of fast-twitch but oxidative IIx fibers without increasing type I fibers (18). Similarly, activated PPARδ, which is known to associate with PGC-1, specifically increases type I fibers (29).

In *Myoz1*-deficient mice, the fiber type and endurance phenotype appear to be mediated via the phosphatase calcineurin, which, besides the PGC-1/PPAR axis, determines muscle fiber specificity. Activated calcineurin promotes a fiber type shift toward slower, more oxidative fibers (1, 3, 4, 7, 8, 31). Here we show that calsarcin-2 inhibits calcineurin activity in muscle cells in vitro. Conversely, the lack of calsarcin-2 in striated muscles led to a significant increase in calcineurin/NFAT activity. Interestingly, *Myoz1*-deficient mice also reveal enhanced muscle regeneration after myotoxic injury, similar to mice overexpressing calcineurin in striated muscle–specific fashion (25).

Consistent with the effects observed in mice with muscle-specific overexpression of activated calcineurin (7), the *Myoz1*-deficient

cantly greater abundance, 158.1%, of nuclear NFATc4 in *Myoz1* KO gastrocnemius compared with that of WT (Figure 7D). Taken together, these data support the notion that calsarcin-2 represents an endogenous inhibitor of calcineurin/NFAT signaling. In turn, when calsarcin-2 is absent, calcineurin activity is enhanced.

Enhanced muscle regeneration in Myoz1-deficient mice. Recently it was reported that activated calcineurin has beneficial effects on skeletal muscle regeneration in vivo (25), while pharmacological inhibition of calcineurin led to a delayed regeneration process (26, 27). Given our hypothesis that deficiency for calsarcin-2 leads to release of inhibition of calcineurin activity, one might predict enhanced muscle regeneration in *Myoz1* KO mice. We thus subjected *Myoz1*-deficient and WT mice to unilateral cardiotoxin injection into the tibialis anterior, with the contralateral muscle serving as a control. After 4 days, *Myoz1* KO muscles already showed enhanced regeneration, such as the formation of new muscles fibers (Figure 8A) and an increase in cell proliferation as measured by BrdU incorporation ($n = 4$ animals, $P = 0.015$; Figure 8, B and C). After 6 days, this effect was still observed (Figure 8D). We consistently detected a significantly attenuated weight loss of tibialis anterior muscle in *Myoz1* KO compared with WT mice (71.2% in WT vs. 87.4% in KO mice, $P = 0.029$; Figure 8E). Moreover, *Myoz1* KO mice showed a higher cell surface area recovery (42.2% in WT vs. 64.8% in *Myoz1* KO mice, $P < 0.0001$; Figure 8F) and a decreased area of
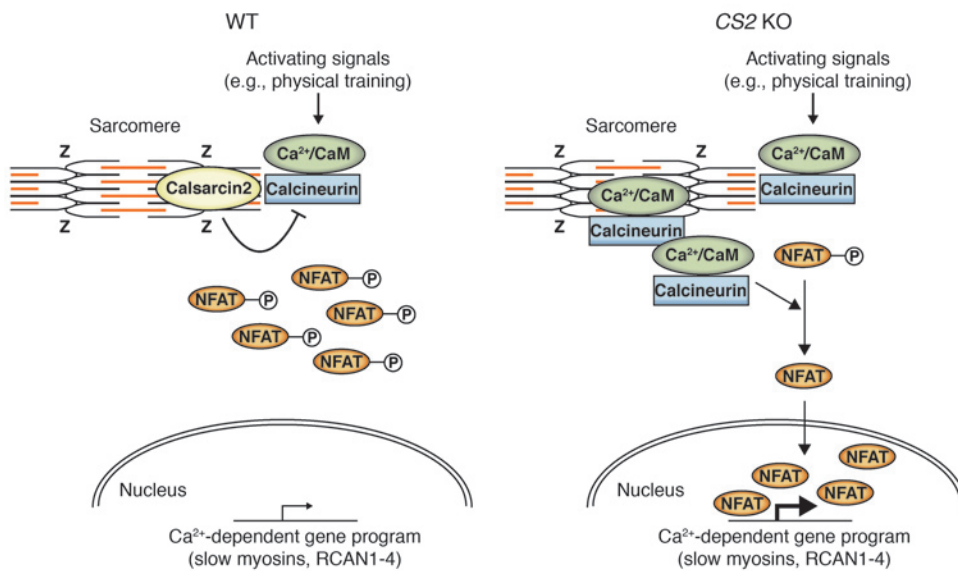
Figure 9
Schematic model depicting calsarcin-2 inhibition of calcineurin activity. In WT skeletal muscle, calsarcin-2 is localized to the Z-disc and inhibits calcineurin activity. Phosphorylated NFAT remains in the cytoplasm. In *Myoz1* KO skeletal muscle, calcineurin dephosphorylates NFAT with consequent nuclear translocation and activation of the calcium-dependent gene program.

skeletal muscle displays an increase in slow-twitch, oxidative fibers. However, the phenotype of *Myoz1*-deficient mice reveals additional features, such as an increase in type I fibers in the slow-twitch soleus muscle, although calsarcin-2 is not expressed in these fibers. This effect might be mediated by a shift from type II fibers, which account for approximately 40%–60% of the soleus (32). In contrast, in fast-twitch fiber–dominant muscles such as the gastrocnemius, the myofiber transition was confined to type IIa fibers without an increased switch toward type I fibers. Likewise, the fast-twitch muscle weight reduction resembled the phenotype observed in the gastrocnemius from calcineurin transgenic mice (33). In *Myoz1* KO mice, the gastrocnemius showed no significant increase of type I fibers compared with WT mice. In contrast, in mice overexpressing activated calcineurin in a muscle-specific fashion, both the number of type I fibers and the weight of the soleus increased (33).

Upregulation of slow, oxidative genes in skeletal muscle promotes fatigue resistance and produces an endurance phenotype (19, 29, 34, 35). Recently we showed that overexpression of activated MEF2 (MEF2C-VP16), a transcription factor that has been shown to associate with NFAT (36), increases the number of slow-twitch fibers as well as the slow-twitch fiber–specific contractile proteins, troponin I and myoglobin. Similar to the *Myoz1*-deficient mice, the MEF2C-VP16 transgenic mice displayed an increase in running time and distance, suggesting that activation of MEF2 is sufficient to enhance skeletal muscle oxidative capacity (37). In addition, in transgenic mice, skeletal muscle overexpression of PKD1, a kinase that phosphorylates class II HDACs and releases repression of MEF2 activity, resulted in an increase in oxidative gene expression and fatigue resistance (38). These studies show that the activation of MEF2, a transcription factor, promotes slow-twitch, oxidative gene expression, resulting in fatigue-resistant skeletal muscle.

Although calcineurin is known to induce the slow-twitch muscle program, to our knowledge it has not been previously shown that an animal model with augmented calcineurin activity actually displays an increase in endurance capacity. Interestingly, the only other mouse model in which a loss-of-function approach led to an increase in exercise capacity is the genetic ablation of another Z-disc protein, α–actinin-3 (34). Similar to *Myoz1*-deficient mice,

mice lacking actinin-3 display a significant increase in endurance and performance, accompanied by an increase in oxidative metabolism in skeletal muscle. While the exact molecular mechanism of the shift toward a more oxidative metabolism in the latter model remains elusive, it is noteworthy that a human polymorphism in the *actinin-3* gene results in the complete absence of this protein in about 18% of the healthy population (39). Remarkably, the lack of actinin-3 is significantly associated with an elite athlete status in humans (40). Similar to calsarcin-2, the expression of α–actinin-3 is restricted to type II skeletal muscle fibers (41). Moreover, α–actinin-3 directly interacts with calsarcin-2 (9). It is thus intriguing to speculate that the effects of α–actinin-3 deficiency on exercise performance are mediated, at least in part, via altered calcineurin/calsarcin/NFAT signaling. While no differences in α–actinin-2 and -3 expression levels were observed in *Myoz1*-deficient animals (Supplemental Figure 4), it is conceivable that calsarcin-2 acts downstream of α–actinin-3. Nevertheless, we cannot exclude that calsarcin-2 as well as α–actinin-3 also modulate other molecular pathways.

In summary, we conclude that calsarcin-2 modulates exercise performance in vivo via regulation of calcineurin/NFAT activity and subsequently the fiber type composition of skeletal muscle. Elimination of calsarcin-2, an endogenous calcineurin inhibitor, from skeletal muscle increases sarcomeric calcineurin activity and results in enhanced exercise capability.

Methods

Gene targeting and genotyping. A 129s6/SvEvTAC mouse genomic BAC library (BACPAC Resources) was screened for *Myoz1* utilizing mouse calsarcin-2 cDNA as a probe. Six independent *Myoz1*-containing genomic clones were mapped, partially sequenced, and used as templates for PCR-mediated amplification of the 5′ and 3′ arms. We designed the targeting vector to replace exon 2 (containing the translation start site) and exon 3. The 5′ arm contained 1.8 kb of the *Myoz1* promoter, exon 1, and intron 1, whereas the 3′ arm contained 5.5 kb of intron 3, exon 4, intron 4, and exon 5. A lacZ reporter cDNA and a neomycin-resistance cassette under control of the phosphoglycerate kinase (*Pgk*) promoter were fused to the 5′-untranslated *Myoz1* sequences contained in the 5′ arm of the targeting vector, placing the lacZ reporter gene under control of the endogenous *Myoz1* promoter. The targeting vector was linearized and electroporated into mouse embry-

onic stem cells of 129Sv origin. Correctly targeted embryonic stem cell clones (identified by Southern blotting using both 5′ and 3′ probes after an EcoRI digestion) were injected into blastocysts derived from C57BL/J mice. Chimeric mice obtained from these blastocyst injections were bred with C57BL/J mice to obtain heterozygous mice that carry the targeted *Myoz1* locus in their germline. Subsequent genotyping was performed by Southern blotting and PCR. Primers for Southern probes were neoF, 5′-GATGCGGTGGGCTCTATGGCTTCTGAGGC-3′; Myoz1F, 5′-GCT-CAGGCCTGAACCTGGGCAAGAAG-3′; and Myoz1R, 5′-GTATGGTCCT-CATGCCTGCACGTGC-3′.

PCR was conducted as a multiplex PCR leading to a 230-bp band (targeted allele) and/or a 400-bp band (WT allele). All subsequent experiments were carried out in the mixed C57BL6/J background. Transgenic animal experiments and animal handling were performed according to the institutional guidelines of the University of Heidelberg and were approved by the animal experiment review board of the government of the state of Baden-Württemberg, Germany. Mice were maintained in a specific pathogen–free environment on a standard rodent chow diet with 12-hour light/12-hour dark cycles. All animals analyzed were adult males (unless stated otherwise) with no significant age differences between genotypes.

Voluntary running wheel analysis. For running experiments, mice were individually housed in cages equipped with voluntary running wheels. Animals were maintained on 12-hour light/12-hour dark cycles, and wheel running activity was monitored continuously with a Sigma-Aldrich data acquisition system for a total of 21 days.

Treadmill analysis. Exercise capacity of mice was measured on a motor-driven treadmill (TSE Systems) following at least 3 days of acclimatization (10% incline, 10 minutes at 10 m/min, subsequent increase of additional 2 m/min each 2 minutes, ending after 20 minutes). Data acquisition was achieved using settings at 10% incline for 10 minutes (10 m/min) and then at an increase of an additional 2 m/min every 2 minutes (+0.033 m/s) until exhaustion.

Assessment of diaphragm muscle function in vitro. Mice were euthanized with isofluorane, and hearts and lungs were rapidly excised. The empty chest was rinsed with ice-cold modified Krebs-Henseleit (K-H) buffer solution containing (in mM) Na$^+$, 140.5; K$^+$, 5.1; Mg^{2+}, 1.2; Ca^{2+}, 0.25; Cl$^-$, 124.9; SO$_4^{2-}$, 1.2; PO$_4^{3-}$, 2.0; HCO$_3^-$, 20; glucose, 10; butanedione monoxime (BDM), 20, pH 7.4. A ring of the chest wall with the diaphragm attached was excised and cleared from blood in ice-cold K-H buffer solution. Longitudinal muscle strips of 0.8–1 mm in width were dissected from the left posterior quadrant of the diaphragm such that a piece of the adjacent rib was on one end and a piece of the tendinous center of the diaphragm was on the other end. Preparations were mounted isometrically between a wire loop connected to a force transducer (Scientific Instruments) and a hook connected to a micrometer drive for length adjustment and superfused at 37°C with K-H solution equilibrated with 95% O$_2$/5% CO$_2$. The solution was replaced with BDM-free K-H solution containing Ca^{2+} at 1.25 mmol/l, and electrical field stimulation was initiated at 1 Hz using biphasic pulses of 4 ms duration and 5 V amplitude (Stimulator STIM1; Scientific Instruments). Preparations were stretched to a passive tension of 1 mN/mm² and allowed to functionally stabilize for 30 minutes. Trains of electrical stimuli (3 s in 10-Hz increments; range, 10–120 Hz) were applied once per minute, and the force response was recorded on a computer using LabView (National Instruments). After another 30-min period for recovery, a fatigue test was initiated consisting of 100 repetitive trains of stimuli at 100 Hz, 250 ms duration, 1/s, during which tetanic force and its decline due to fatigue were recorded. All force values were normalized to the cross-sectional area of the respective muscle preparations (mN/mm²).

Tissue culture and luciferase assays. C2C12 myoblasts were stably transfected using the pHTS NFAT reporter vector (Biomyx) carrying a luciferase expression cassette under control of 4 NFAT enhancer sites. NFAT-luc

C2C12 cells were maintained in DMEM containing 10% FBS, 2 mM L-glutamine, and penicillin/streptomycin. Twenty-four hours before measurements, cells were transfected with 1.2 μg of expression plasmids encoding calsarcin-2 and constitutively active or full-length calcineurin A using the FuGENE HD reagent (Roche Applied Science). All experiments were conducted in duplicate and repeated at least 3 times. Promega's dual luciferase assays were performed according to the manufacturer's instructions. All results were normalized to a simultaneously transfected pRL-TK renilla luciferase. Stimulation of cells was carried out using PMA (40 ng/ml) and ionomycin (2 μM, both from Sigma-Aldrich).

RNA isolation and quantitative real-time PCR. Total RNA from freshly harvested mouse muscles was isolated using TRIzol reagent (Invitrogen) following the manufacturer's instructions after tissue homogenization with an Ultra-Turrax tissue separator (IKA). Before reverse transcription, DNase digestion and purification of RNA was carried out on RNeasy kit columns (QIAGEN). Subsequently, DNase-digested total RNA was transcribed into cDNA using the Superscript III First-Strand kit (Invitrogen). For real-time PCR, the Platinum SYBR Green qPCR SuperMix-UDG System (Invitrogen) was used in an ABI Prism 7700 Sequence Detection System (PerkinElmer). PCR amplifications were performed using the following protocol: 2 minutes at 95°C, followed by a total of 40 temperature cycles (15 seconds at 95°C, 15 seconds at 57°C, and 1 minute at 72°C). 18S rRNA primers served as an internal standard.

Protein preparation and western blot analysis. Muscle samples of animals were harvested, immediately transferred into RIPA buffer containing 10 mmol/l Tris, 15 mmol/l EDTA pH 7.5, 1% NP-40 (vol/vol), 0.5% sodium deoxycholate (wt/vol), 0.1% SDS (wt/vol) (Sigma-Aldrich), and protease inhibitor cocktail tablets (Roche Applied Science) and homogenized using an Ultra-Turrax tissue separator (IKA). For conventional western blotting, homogenates were resolved by SDS-PAGE, transferred to a Westran PVDF membrane (Schleicher & Schüll), and immunoblotted with the primary antibody (monoclonal anti–calsarcin-2 [BD Biosciences], 1:5,000, or specific polyclonal anti–actinin-2 or anti–actinin-3, 1:500 each, kind gifts from A.H. Beggs, Harvard Medical School, Boston, Massachusetts, USA; refs. 39, 41). The application of the primary antibodies was followed by incubation with the respective anti-mouse or anti-rabbit HRP-coupled secondary antibody (1:10,000; Santa Cruz Biotechnology Inc.). Visualization was achieved using a chemoluminescence kit (Amersham Biosciences).

In additional experiments, the Li-Cor Odyssey detection system was used. Muscle homogenates were resolved by SDS-PAGE, transferred to an Immobilon FL membrane (Millipore), and analyzed with the primary antibodies polyclonal rabbit anti–calsarcin-1 (1:1,000) (9), polyclonal rabbit anti–MCIP-1 (anti-RCAN1, 1:1,000) (42), or polyclonal rabbit anti-NFATc4 (H-74, 1:200; Santa Cruz Biotechnology Inc.). After staining with the secondary antibody IRDye 800CW Goat Anti-Rabbit IgG (LI-COR Biosciences), bands were visualized with a LI-COR Biosciences infrared imager (Odyssey). Quantitative densitometric analysis was performed using Odyssey version 1.2 infrared imaging software.

Coimmunoprecipitation. HEK 293T cells were maintained in DMEM medium containing 10% FBS, 2 mM L-glutamine, and penicillin/streptomycin. Cells (1 × 10⁶) were transfected with 7.5 μg of expression plasmids for α–actinin-2 (ACTN2) and α–actinin-3 (ACTN3) as well as a HA-tagged human calsarcin-2 construct (HA–calsarcin-2) using FuGENE HD reagent (Roche Applied Biosciences). Two days after transfection, cells were harvested in RIPA buffer containing 10 mM Tris (pH 7.5), 15 mM EDTA, 0.5% sodium deoxycholate, 1% NP-40, 1 mM DTT, 0.1% SDS, and the Complete protease inhibitor cocktail (Roche Applied Bioscience). HA–CS-2 was immunoprecipitated for 2–3 hours at 4°C using HA-coupled beads as recommended by the manufacturer (monoclonal anti-HA; Sigma-Aldrich). Subsequently, the pellet was washed with RIPA buffer and subjected to SDS-PAGE, followed by transfer

to polyvinylidene membranes and immunoblotting using specific polyclonal anti–actinin-2 and anti–actinin-3 (1:500 each) as well as the monoclonal anti–calsarcin-2 antibody (1:5,000; BD Biosciences).

Histology and immunofluorescence analyses. For cryosections, harvested muscle tissue was snap frozen in liquid nitrogen and embedded in cryomedium. Cryosections from WT and *Myoz1* KO skeletal muscle were air dried and fixed in 4% ice-cold (–20°C) acetone for 10 minutes, followed by 3 washes with PBS. For histological analyses, sections were stained with H&E or van Gieson stain to visualize tissue architecture and potential fibrosis, respectively.

For immunofluorescence experiments, sections were permeabilized with 0.3% Triton X-100 (Sigma-Aldrich) and blocked in 5% BSA in PBS for 1 hour. Primary antibodies were incubated for 1 hour at room temperature or overnight at 4°C. For primary antibodies, we used several monoclonal anti-myosin antibodies (skeletal, slow, clone NOQ7.5.4D, 1:2,000 [Sigma-Aldrich]; monoclonal anti-skeletal myosin fast, IgG1, 1:250, clone MY-32 [Sigma-Aldrich]; mouse hybridoma SC-71 [anti-MHC IIa], DSMZ no. ACC217; and mouse hybridoma BF-F3 [anti-MHC IIb], DSMZ no. ACC212. For secondary antibodies, fluorescein-coupled anti-rabbit antibody (Vector Laboratories) and Cy3-coupled anti-mouse antibody (Dianova:115-165-003) were incubated at a dilution of 1:200 for 1 hour. Lectin stainings were carried out using lectin from *Triticum vulgaris* (wheat) as FITC conjugate L4985 (Sigma-Aldrich) according to the manufacturer's protocol. The cross-sectional areas of muscle fibers were determined using ImageJ software, version 1.62.

For β-galactosidase staining, dissected muscles and hearts were fixed with 2% paraformaldehyde/0.1% glutaraldehyde in PBS on ice for 30–45 minutes, followed by washing and X-gal staining (5 mM ferrocyanide, 5 mM ferricyanide, 2 mM $MgCl_2$, 1 mg/ml X-gal, 0.01% sodium deoxycholate, 0.02% NP-40) for 6–12 hours.

SDH stainings on cryosections were carried out using a 0.2 M phosphate buffer at pH 7.6. For staining, 270 mg succinic acid and 10 mg nitro blue tetrazolium (NBT) were freshly dissolved in 10 ml phosphate buffer and incubated with sections for 1 hour. After 3 washings with water, sections were photomicrographed.

Regeneration of skeletal muscle after cytotoxic injury. A single injection of 50 μl of 10 μM cardiotoxin (from *Naja naja atra*; Sigma-Aldrich) was administered into the tibialis anterior. As a negative control, 0.9% saline solution was injected into the contralateral extremity under general anesthesia (100 mg ketamine/kg and 15 mg xylazine/kg). During and after the procedure, buprenorphin was administered as an analgesia. Briefly, the skin of the hindlimb was disinfected with 70% vol/vol ethanol. After palpation of the tibialis anterior muscle, cardiotoxin or saline was injected. For analyses at days 4 and 6 after injection, mice were sacrificed and muscles were excised and subjected to standard immunofluorescence and light microscopy techniques, as described above. For BrdU incorporation studies, 5-/bromodeoxyuridine (1 mg/kg; ICN Biochemicals) was injected intraperitoneally. After 6 hours mice were sacrificed and muscles were excised and further processed. The primary antibody was a monoclonal anti-BrdU (1:100; Roche Applied Science). A FITC-conjugated anti-mouse antibody was used as the secondary antibody (1:10,000; Vectashield).

Electron microscopy. Muscles from control and calsarcin-2–deficient mice were dissected and fixed in 4% glutaraldehyde in 0.1 M cacodylate buffer. Striated muscle tissue was rinsed with 0.1 M cacodylate buffer. The tissue was then postfixed and stained with 1% osmium tetroxide in 0.1 M cacodylate buffer and incubated with uranyl acetate. The dehydration step was carried out with increasing concentrations of ethanol. The tissues were subsequently rinsed with acetone oxide and embedded using EPON (glycid ether 100; Serva). After hardening, longitudinal thin sections were counterstained with uranyl acetate and lead citrate and examined on an electron microscope. The photomicrographs were taken at a magnification of ×19,000. Z-disc width was measured in 100 longitudinally aligned Z-discs from 4 animals per genotype.

Statistics. All results are shown as the mean ± SEM unless stated otherwise. Statistical analyses of the data were carried out using the Student's *t* test (2-sided). When necessary, 1- or 2-way ANOVA (followed by Student-Newman-Keuls post-hoc tests when appropriate) was applied. *P* values of less than 0.05 were considered statistically significant.

Address correspondence to: Norbert Frey, Department of Internal Medicine III, University of Heidelberg, Im Neuenheimer Feld 410, D-69120 Heidelberg, Germany. Phone: 49-6221-566877; Fax: 49-6221-564866; E-mail: norbert.frey@med.uni-heidelberg.de. Or to: Eric N. Olson, Department of Molecular Biology, University of Texas Medical Center, 5323 Harry Hines Blvd., Dallas, Texas 75390-9148, USA. Phone: (214) 648-1187; Fax: (214) 648-1196; E-mail: eric.olson@utsouthwestern.edu.

Tomasa Barrientos's present address is: Department of Pharmacology and Cancer Biology, Duke University, Durham, North Carolina, USA.

Norbert Frey, Derk Frank, and Stefanie Lippl contributed equally to this work.

1. Bassel-Duby, R., and Olson, E.N. 2006. Signaling pathways in skeletal muscle remodeling. *Annu. Rev. Biochem.* **75**:19–37.
2. Dolmetsch, R.E., Lewis, R.S., Goodnow, C.C., and Healy, J.I. 1997. Differential activation of transcription factors induced by Ca2+ response amplitude and duration. *Nature.* **386**:855–858.
3. Bassel-Duby, R., and Olson, E.N. 2003. Role of calcineurin in striated muscle: development, adaptation, and disease. *Biochem. Biophys. Res. Commun.* **311**:1133–1141.
4. Schiaffino, S., Sandri, M., and Murgia, M. 2007. Activity-dependent signaling pathways controlling muscle diversity and plasticity. *Physiology (Bethesda).* **22**:269–278.
5. Chin, E.R., et al. 1998. A calcineurin-dependent transcriptional pathway controls skeletal muscle fiber type. *Genes Dev.* **12**:2499–2509.
6. Delling, U., et al. 2000. A calcineurin-NFATc3-dependent pathway regulates skeletal muscle differentiation and slow myosin heavy-chain expression. *Mol. Cell. Biol.* **20**:6600–6611.
7. Naya, F.J., et al. 2000. Stimulation of slow skeletal muscle fiber gene expression by calcineurin in vivo. *J. Biol. Chem.* **275**:4545–4548.
8. Parsons, S.A., et al. 2004. Genetic loss of calcineurin blocks mechanical overload-induced skeletal muscle fiber type switching but not hypertrophy.
9. *J. Biol. Chem.* **279**:26192–26200.
10. Frey, N., Richardson, J.A., and Olson, E.N. 2000. Calsarcins, a novel family of sarcomeric calcineurin-binding proteins. *Proc. Natl. Acad. Sci. U. S. A.* **97**:14632–14637.
11. Frank, D., Kuhn, C., Katus, H.A., and Frey, N. 2006. The sarcomeric Z-disc: a nodal point in signalling and disease. *J. Mol. Med.* **84**:446–468.
12. Takada, F., et al. 2001. Myozenin: an alpha-actinin- and gamma-filamin-binding protein of skeletal muscle Z lines. *Proc. Natl. Acad. Sci. U. S. A.* **98**:1595–1600.
13. Faulkner, G., et al. 2000. FATZ, a filamin-, actinin-, and telethonin-binding protein of the Z-disc of skeletal muscle. *J. Biol. Chem.* **275**:41234–41242.

13. Frey, N., and Olson, E.N. 2002. Calsarcin-3, a novel skeletal muscle-specific member of the calsarcin family, interacts with multiple Z-disc proteins. *J. Biol. Chem.* **277**:13998–14004.

14. Gontier, Y., et al. 2005. The Z-disc proteins myotilin and FATZ-1 interact with each other and are connected to the sarcolemma via muscle-specific filamins. *J. Cell. Sci.* **118**:3739–3749.

15. Frey, N., et al. 2004. Mice lacking calsarcin-1 are sensitized to calcineurin signaling and show accelerated cardiomyopathy in response to pathological biomechanical stress. *Nat. Med.* **10**:1336–1343.

16. Frank, D., et al. 2007. Calsarcin-1 protects against angiotensin-II induced cardiac hypertrophy. *Circulation.* **116**:2587–2596.

17. Glass, D.J. 2003. Molecular mechanisms modulating muscle mass. *Trends Mol. Med.* **9**:344–350.

18. Arany, Z., et al. 2007. The transcriptional coactivator PGC-1beta drives the formation of oxidative type IIX fibers in skeletal muscle. *Cell Metab.* **5**:35–46.

19. Booth, F.W., and Thomason, D.B. 1991. Molecular and cellular adaptation of muscle in response to exercise: perspectives of various models. *Physiol. Rev.* **71**:541–585.

20. Schiaffino, S., and Reggiani, C. 1996. Molecular diversity of myofibrillar proteins: gene regulation and functional significance. *Physiol. Rev.* **76**:371–423.

21. Molkentin, J.D., et al. 1998. A calcineurin-dependent transcriptional pathway for cardiac hypertrophy. *Cell.* **93**:215–228.

22. Davies, K.J., et al. 2007. Renaming the DSCR1/Adapt78 gene family as RCAN: regulators of calcineurin. *FASEB J.* **21**:3023–3028.

23. Yang, J., et al. 2000. Independent signals control expression of the calcineurin inhibitory proteins MCIP1 and MCIP2 in striated muscles. *Circ. Res.* **87**:E61–E68.

24. Crabtree, G.R., and Olson, E.N. 2002. NFAT signaling: choreographing the social lives of cells. *Cell.* **109**(Suppl.):S67–S79.

25. Stupka, N., Schertzer, J.D., Bassel-Duby, R., Olson, E.N., and Lynch, G.S. 2007. Calcineurin-A alpha activation enhances the structure and function of regenerating muscles after myotoxic injury. *Am. J. Physiol. Regul. Integr. Comp. Physiol.* **293**:R686–R694.

26. Abbott, K.L., Friday, B.B., Thaloor, D., Murphy, T.J., and Pavlath, G.K. 1998. Activation and cellular localization of the cyclosporine A-sensitive transcription factor NF-AT in skeletal muscle cells. *Mol. Biol. Cell.* **9**:2905–2916.

27. Sakuma, K., et al. 2003. Calcineurin is a potent regulator for skeletal muscle regeneration by association with NFATc1 and GATA-2. *Acta Neuropathol.* **105**:271–280.

28. Lin, J., et al. 2002. Transcriptional co-activator PGC-1 alpha drives the formation of slow-twitch muscle fibres. *Nature.* **418**:797–801.

29. Wang, Y.X., et al. 2004. Regulation of muscle fiber type and running endurance by PPARdelta. *PLoS Biol.* **2**:e294.

30. Arany, Z., et al. 2005. Transcriptional coactivator PGC-1 alpha controls the energy state and contractile function of cardiac muscle. *Cell Metab.* **1**:259–271.

31. Parsons, S.A., Wilkins, B.J., Bueno, O.F., and Molkentin, J.D. 2003. Altered skeletal muscle phenotypes in calcineurin Aalpha and Abeta gene-targeted mice. *Mol. Cell. Biol.* **23**:4331–4343.

32. Dapp, C., Schmutz, S., Hoppeler, H., and Fluck, M. 2004. Transcriptional reprogramming and ultrastructure during atrophy and recovery of mouse soleus muscle. *Physiol. Genomics.* **20**:97–107.

33. Talmadge, R.J., et al. 2004. Calcineurin activation influences muscle phenotype in a muscle-specific fashion. *BMC Cell Biol.* **5**:28.

34. MacArthur, D.G., et al. 2007. Loss of ACTN3 gene function alters mouse muscle metabolism and shows evidence of positive selection in humans. *Nat. Genet.* **39**:1261–1265.

35. Wu, H., et al. 2002. Regulation of mitochondrial biogenesis in skeletal muscle by CaMK. *Science.* **296**:349–352.

36. Wu, H., et al. 2001. Activation of MEF2 by muscle activity is mediated through a calcineurin-dependent pathway. *EMBO J.* **20**:6414–6423.

37. Potthoff, M.J., et al. 2007. Histone deacetylase degradation and MEF2 activation promote the formation of slow-twitch myofibers. *J. Clin. Invest.* **117**:2459–2467.

38. Kim, M., et al. 2008. Protein kinase D1 stimulates MEF2 activity in skeletal muscle and enhances performance. *Mol. Cell. Biol.* **28**:3600–3609.

39. North, K.N., et al. 1999. A common nonsense mutation results in alpha-actinin-3 deficiency in the general population. *Nat. Genet.* **21**:353–354.

40. Yang, N., et al. 2003. ACTN3 genotype is associated with human elite athletic performance. *Am. J. Hum. Genet.* **73**:627–631.

41. North, K.N., and Beggs, A.H. 1996. Deficiency of a skeletal muscle isoform of alpha-actinin (alpha-actinin-3) in merosin-positive congenital muscular dystrophy. *Neuromuscul. Disord.* **6**:229–235.

42. Bush, E., et al. 2004. A small molecular activator of cardiac hypertrophy uncovered in a chemical screen for modifiers of the calcineurin signaling pathway. *Proc. Natl. Acad. Sci. U. S. A.* **101**:2870–2875.